Evaluation of the Concrete of the Oyster River Durham Falls Dam Concrete

Final Report

to

David Cedarholm, PE

Durham Town Engineer

and

Bethel Stephens, P.E.

and

Robert S. Stephens, PE, PG

Stephens Associates Consulting Engineers, LLC

by

Dr. David Gress Ph.D., P.E.

Consulting Engineer

Portsmouth, NH

March 25, 2010

TESTING PROTOCOL

The Oyster River Durham Falls Dam testing protocol consisted of visual observation of the Dam, taking audio soundings, coring of selected areas, and laboratory evaluation of the concrete obtained during coring. The laboratory evaluation of the cores consisted of performing conventional hardened properties testing (compressive and splitting tension strength, unit weight, and elastic modulus), cutting and polishing for microscopic evaluation, making thin sections for detailed petrographic analysis and coating new fractured surfaces for testing for specific materials related distress.

TESTING RESULTS

Visual Analysis

The visual analysis of the concrete was consistent with the findings of the recent report, Dam Evaluation Report Oyster River Dam, SA Project No. 075-07-003, March 17, 2009. In general the concrete was found to be overall in good condition for its age. There are areas where erosion of the concrete was noted such as the top crest of the spillway, the downstream face of the ribs and portions of the right abutment. The right side abutment, especially on the downstream face showed signs of cracking and effloresce of what appeared to be calcium hydroxide.

Audio Soundings

Soundings were taken over the surface of the dam that would have been expected to have gone through freezing and thawing cycles. This was accomplished by using a geological hammer to tap the surface being evaluated while listing to the ring of the sound produced. Sharp high pitch rings are consistent with high quality concrete whereas thuds and lower pitch rings suggest areas that have lower quality concrete and/or areas that have delaminated. In general the concrete was found to be in relatively good condition. There were some minor areas on the upstream portion of the crest where the 1974 bonded overlay had delaminated. There were also some areas in the interior downstream components of cells 1 and 2 (including their ribs) which definitely were of lower quality concrete. The right abutment also had areas that were of lower quality concrete.

Cores

Cores were taken at the approximate locations as shown in Table 1. Cores #1 through #4 were four inches in diameter and cores #5 through #13 were six inches in diameter. It was decided to increase the size to six inches due to the relatively large maximum aggregate size in excess of 2” so as not to bias the laboratory testing results.

Laboratory Testing

Physical Tests

Cores were selected for compressive strength testing (ASTM C 39/C 39M – 01, Standard Test Method for Compressive Strength of Cylindrical Concrete Specimens), elastic modulus (ASTM C 469 – 02, Standard Test Method for Static Modulus of Elasticity and Poisson's Ratio of Concrete in Compression), splitting tension (ASTM C 496 – 96, Standard Test Method for Splitting Tensile Strength of Cylindrical Concrete Specimens) and unit weight and absorption **(**ASTM C 127 – 01 Standard Test Method for Density, Relative Density (Specific Gravity), and Absorption of Coarse Aggregate).

Physical tests performed on the cores are presented in Table 2.

Splitting Tension

The results of the splitting tension testing are presented in Table 3. The tensile strengths except for the #2 original concrete were much lower than expected. The average for the original concrete, identified by "Old" was 380 psi. The strength of the 1974 overlay was 330 psi however this is based on only one sample. Overall these data show the splitting tensile strength to be much less than expected based on the visual analysis of the concrete suggesting the possible existence of micro cracks in the concrete.

Compression Strength

The compression strength testing data are presented in Table 4. As was expected the strengths were relatively high with an average for the original concrete of 5780 psi.

Compression and Tension

A comparison between compression strength and tensile strength gives an excellent indication of micro cracking. A Materials Related Distress (MRD) typically affects the relationship between the two strength properties by reducing the tensile strength. The ratio of tensile strength to compression strength is shown in Table 5. These data show the tensile strength to be about 10 percent of the compressive strength for core #2 and about 5 to 6 percent for cores #3 and #8. The concrete in an undisturbed state would be expected to have a ratio of between 7 and 8 percent. The 10 percent value is higher and the 5/6 is exceptionally lower than what would be expected. Such variation gives a strong indication of the presence of a MRD.

Unit Weight

Table 6 shows the unit weight of the original concrete to be 142.2 lbs/ft^3 for the newer concrete and 139.4 lbs/ft^3 for the older original concrete. The absorptions were 2.4 percent for the newer concrete and 3.6 percent for the older original concrete. The absorption data are lower than what would be expected.

- ***Elastic Modulus***

The elastic moduli data of the concrete are presented in Table 7. The average elastic modulus for the concrete obtained from the upstream face (#4 Top) was 4.13 $x10^6$ psi and the average rib (#4 Bottom & #7) was 3.77 $x10^6$ psi. Using the compressive strength and the unit weight it is possible to estimate the elastic modulus of a concrete based on American Concrete Institute criteria. Using the ACI equation the estimated elastic moduli were 4.53 $x10^6$ psi for the upstream face and an average of 3.96 $x10^6$ psi for the rib sections. Ratios of the actual to the predicted elastic moduli ranged from 0.913 for the upstream face to an average of 0.955 for the rib sections. These data show as with the tensile strength data that there is significant evidence of a Materials Related Distress.

Petrographic Testing

Selected cores were cut and polished for visual observation under a standard binocular microscope. A technique to enhance the visual identification of cracks was performed on several polished sections by coating them with low viscosity epoxy impregnated with an ultra violent fluorescing pigment. Other tests conducted included, applying the new fractured surface of the splitting tension and compression specimens with a solution of Uranyl Acetate dihydrate then viewing under ultra violet light to evaluate for the presence of Alkali Silica Reaction (ASR) and making thin sections to view the concrete on a petrographic microscope. The tests conducted on the cores are as presented in Table 2.

Polished Sections

Selected cores were cut using a diamond blade then polished on a lapidary wheel using various grit sizes. Figure 1 shows the upper portion of the concrete from the 1974 rehabilitation. Cracking of the concrete is shown in a close up of section A in Figure 2. Micro cracks were apparent in Figure 3, the same sample as in Figure 1, after epoxy was applied with the Ultra Violent (UV) pigment. The surface was repolished to enhance the presence of cracks when viewed under UV light. These cracks are most likely due to Freeze Thaw damage.

Figure 4 shows the concrete of the spillway crest obtained in core # 5. Sections B, C, D, and F show four different concretes. Section B is the 1974 repair concrete, C is a layer of mortar that was applied to achieve a bond between the old original concrete shown in section D and the new concrete in section B. The lower portion shown by section F contains very large aggregate and is well compacted compared to the concrete of section D which has little coarse aggregate and shows poor compaction. This concrete was apparently mixed on site and hand placed which would be the expected procedure in 1913. The original concrete as seen on the lower portion consists of a natural glacial gravel material most likely obtained in the near vicinity of the Dam. It contains various minerals mostly of igneous origin with a maximum aggregate size of approximately 2." Several of the large aggregate pieces consisted of a deteriorated granite that was so weak it came apart during the polishing process as noted by the small pieces of mica scattered throughout the concrete. Figure 5 shows a close up of section A which contains a crack, most likely from freeze thaw damage. It also contains several pores filled with a white powder deposit. Figure 6 shows a close up of the mortar applied to enhance the bond at the old and new

interface. This layer was poorly compacted as shown by the voids at the old interface as well as in the matrix of the layer. Several other voids containing the white powder are shown on the close up view of section E in Figure 7. These voids appear to be interconnected by a crack that initiated in the aggregate particle on the right side of figure 7.

The polished section of Core #5 was coated with a low viscosity epoxy that was impregnated with an UV fluorescing pigment and repolished so as to visually enhance the micro cracks. Figure 8 shows the polished section coated with the epoxy under UV light. A view of the mid section of the epoxy coated Core #5 under UV light is shown in Figure 9. Micro cracks are visible within the aggregate as well as the paste matrix. Reaction rims are also emphasized by the dark areas on the on the edge of most of the aggregates.

An overall view of the polished section of Core #6 is shown on Figure 10. This shows four different concretes the 1974 repair concrete, the interface mortar, a high entrapped air concrete with little aggregate, and the typical original described above. The surface concrete shows signs of freeze thaw damage as noted by the parallel cracks as shown in the close up view of section a in Figure 11. The mortar interface layer is poorly consolidated and is delaminating at the old concrete interface as shown by Figure 12. Aggregate internal cracking and matrix cracking are shown on the close up view of section C on Figure 13.

Core # 9 obtained horizontally from the rib is shown on Figure 14. This concrete appears more uniform because the core was taken horizontally. If the core was obtained vertically as the previous cores then it would be expected that several placements would be viewed showing variable mixes. Overall this concrete shows cracking and reaction rims as the previous original concrete. Figure 5 shows a close up of section A with cracking within the aggregate particle as well as around it. Figure 14 shows a crack radiating up towards the surface of the concrete originating from an aggregate particle that has expanded as shown in the close up view in Figure 16. Another aggregate particle that has expanded is shown in Figure 17, a close up view of section C. This aggregate is severely cracked due to internal expansion. Reaction rims are also visible on the outside surface of the aggregate. The aggregate particle of section D, shown in Figure 18 has micro cracks. The interface of the aggregate and the paste also shows cracking. The flat like dark line near the right top side of the aggregate particle is a sliver of mica. These small slivers are randomly dispersed throughout the concrete and most likely came from the very weak granite particles that degraded during the mixing and placement of the concrete. A severely cracked aggregate particle is shown in the close up view of section E in Figure 19. This aggregate particle also has a very dark reaction rim. An advanced crack matrix is shown in the close up view of section F of Figure 20.

The polished sample of Core # 12 taken from the downstream face of the right abutment is shown on Figure 21. Many of the aggregate particles have reaction rims as noted in the previous polished sections. Section A shows a highly carbonated area with significant cracking. The polished sample shows massive cracking as noted by the arrows radiating from box B. Extreme swelling of the aggregate is noted by the large gap shown in the aggregate particle in the close up of section C in Figure 23. The area of paste to the left of the particle shows a very large crack, the same width as the aggregate crack, which has filled in with a reaction product. Cracking through and around aggregate particles is shown in the close up view of section D in

Figure 24. Several aggregate particles in this view also show reaction rims. This concrete has undergone significant expansion.

Uranyl Acetate Testing

After the splitting tensile testing was completed the two approximately equal size pieces from each test were evaluated for Alkali Silica Reaction (ASR) by coating one of the two pieces with a solution of Uranyl Acetate Dihydrate and viewing both under an ultraviolet light source (UV). Similarly this procedure was followed for Core # 1, a compression strength sample. Areas that contain ASR gel show a greenish glow. Figures 25 through 28 show the cores that were evaluated for ASR under UV light and normal light. The photograph on the top of the figures is of the samples under normal light.

Core # 1 shown in Figure 25 definitely has signs of ASR as noted by the greenish glow under the UV light source. The concrete placed during the 1974 rehabilitation is shown in Figure 26 and 27. Although not significant, several of the aggregate particles definitely show signs of ASR in the repair concrete. The original concrete definitely shows significant signs of ASR as noted by Core # 8 of Figure 28.

Thin Sections

Thin sections were made so a petrographic analysis of the original concrete could be determined. Core # 13 from the right abutment downstream face was selected for the analysis. The concrete was visually identified as being typical of the concrete observed in the other cores. Two sections were cut for preparing the thin sections. The first was parallel to the wall surface and referred to as the vertical section. The second was taken perpendicular to the surface and referred to as the horizontal section. These thin sections were evaluated using a petrographic microscope.

Figure 29 through Figure 36 are from the vertical section and Figure 37 through Figure 45 are from the horizontal section. Extensive aggregate cracking and deposits of ASR gel are shown on Figure 29. The blue color is from a dye used to emphasize voids and cracks that are empty. When the light source is changed from normal to polarized it is referred to as crossed nicols, this allow for the identification of various crystalline and amorphous materials. For example, Figure 30 shows a dark substance that is amorphous ASR gel by using polarized light. Layered ASR gel is shown in Figure 31. The same view under polarized light shows various layers of crystalline and amorphous ASR gel. The ASR reaction has been active for a long time period as shown by the multiple layers. Figure 33 shows the same area as figures 31 and 32 but under lower magnification. Extreme cracking is noted in the aggregate in Figure 34. The silica from the aggregate combines with alkali and calcium to make the ASR gel as shown deposited in the air void. Ettringite, a mineral with composition $(CaO)_3(Al_2O_3)(CaSO_4)_3 \cdot 32\ H_2O$ is produced naturally within portland cement during initial hydration. When a portland cement system becomes compromised by excessive cracking the Ettringite moves around and is redeposited.

This is referred to as secondary Ettringite. Such is shown by Figures 35 through 38 where the secondary Ettringite has deposited within a crack at the aggregate paste interface. Figure 39 shows cracking through a granite particle due to ASR. Deposits of Ettringite are also indicated on Figure 39, 40 and 41. The crack shown in Figure 41 with the ASR gel gives a good indication of the destructive impact that the reaction has had on the dimensional stability of the concrete. This concrete has definitely expanded and in the process it has undergone excessive cracking as indicated by Figure 42 and 43. Some of these cracks could be associated with freezing and thawing damage. Once a concrete opens up from cracking it becomes vulnerable to other distress mechanisms.

The portland cement used in the construction of the Oyster River Durham Falls Dam was a natural cement made of limestone with a high clay content (argillaceous limestone) from Rosendale, New York. The burn temperature of this cement was much lower than a normal portland cement resulting in a cement different from a normal portland cement. The Rosendale cement would have been expected to have a fast initial set, followed by a very slow and gradual rise in strength. There are always considerable amounts of unhydrated cement resulting in a common identifying feature when the concrete is viewed under a microscope as shown by Figure 44. Another characteristic of the Rosendale cement is the presence of a higher than normal, compared to normal portland cement, percentage of calcium hydroxide as shown in Figure 46.

DISCUSSION

The physical test properties of the Durham Falls Dam show the compressive strengths to be very high with an average strength of approximately 5,780 psi. Compression strength, although universally utilized as a major indicator of concrete quality world wide, is not capable of detecting the presence of ASR.

The tensile strength data, average of 380 psi, show the concrete to be less than what would be expected based on the compressive strengths. The ratio of tensile strength to compressive strength was approximately 5 to 6 percent which is lower than what would be expected. This strongly suggests the concrete is severely cracked internally which was observed in the petrographic evaluation. One core showed a high ratio of 10 percent which is typical of a high quality concrete. Highly variable data such as these are to be expected for a concrete structure that is subject to ASR.

The elastic modulus is an excellent indicator of the presence of micro and macro cracks. The elastic moduli data show a difference between the elastic modulus expected and what was determined on the cores. The ratio of experimental to expected elastic moduli ranged from 91 to 98 percent. This also shows the effect of microcracking. These ratios being less than expected suggests the structural capability of the concrete has been reduced due to MRD.

The Uranyl Acetate testing showed the presence of ASR gel on the cracked faces of the splitting tension samples. Although this test is not by itself a sole indicator of the destructive presence of ASR it does show a significant amount of gel has been produced within the concrete.

The petrographic analysis showed beyond doubt that the concrete has ASR and extensive microcracking and macrocracking has occurred throughout the concrete matrix as well as within the reactive aggregate. Expansion of the old concrete relative to the newer 1974 repair concrete would be expected to cause the bond to fail and/or tensile cracks to occur. Delaminating and tensile cracking were both observed in the repair concrete during the acoustic hammer testing and while viewing the polished sections.

Nothing is known about the remaining potential for continued expansion due to ASR. This was not part of the testing protocol because visually there was no indication that ASR was a major player in the quality of the concrete. If the alkali of the concrete has been consumed ASR can not continue and the present state (dimensional stability) of the concrete would be expected to remain about the same in the future except for the effect of freezing and thawing. On the other hand, if the alkali content of the concrete is high enough then the ASR will continue resulting in increased expansion of the concrete. Further expansion of the concrete will increase microcracking and macrocracking, lower concrete strength, accelerate delaminating and increase surface erosion. The rate of deterioration will increase due to the compounding effect of opening the system to moisture which is required for both the freeze thaw and ASR mechanism to occur. Such a condition would be problematic to the useful service life of the Dam.

SUMMARY

The physical and petrographic testing of the Durham Falls Dam shows the concrete has deteriorated from ASR and freeze thaw. These distresses have decreased the concrete's tensile and elastic properties and will have an impact on the useful serviceability of the Dam. Nothing is known about the remaining ASR expansion potential so the predicted remaining service life is difficult to address. However, it is known that once ASR opens a concrete up by micro and macrocracking then other distresses like freeze thaw can have a major impact. Deterioration increases at an exponential rate because it is easier for water, a key component, to enter the interior of the concrete thus accelerating the distress. This accelerated effect will be first noted on the areas presently showing erosion and cracking.

It is very probable the effective service life of the Oyster River Durham Falls Dam is approaching its economical and useful service life.

RECOMMENDATIONS

It is difficult to make a viable recommendation for the future use of the Oyster River Durham Falls Dam due to lack of knowledge of the remaining ASR potential expansion in the existing concrete. It is recommended that this be determined prior to deciding the future fate of the Dam. If the reaction has not stopped then a conventional rehabilitation, bonding new concrete to the existing, will not be possible. This technique was used in the 1975 rehabilitation strategy and is

the primary cause of the existing delamination and debonding noted during the evaluation. On the other hand, if the reaction has come to completion, it is possible to bond new concrete to the existing concrete making the rehabilitation much more cost effective. The alternative of not being able to bond to the existing concrete would increase the rehabilitation cost to the extent that the cost of removing the dam would be more financially palatable.

Table 1 Core approximate locations

Core	Approximate location
#1	Top of spillway crest in cell 6
#2	Top of spillway crest in cell 6
#3	Top of spillway crest in cell 6
#4	Upstream face through reinforcing steel
#5	Top of spillway crest in cell 5
#6	Top of spillway crest in cell 5
#7	Rib between cell 8 and 7 taken horizontally
#8	Rib between cell 8 and 7 taken horizontally
#9	Rib between cell 5 and 6 taken horizontally
#10	Downstream face of right abutment taken horizontally
#11	Downstream face of right abutment taken horizontally
#12	Downstream face of right abutment taken horizontally
#13	Downstream face of right abutment taken horizontally

Table 2 Core and Sample testing identification

Core	Splitting Tension	Compression strength	Elastic Modulus	Unit weight	Uranyl Acetate	Petrographic		
						Cut and polish	Epoxy impregnate	Thin section
#1		X			X	X	X	
#2	X				X			
#3	X	X			X			
#4 Top		X	x	X		X	X	
#4 Bottom		X	X	X				
#5						X		
#6						X		
#7		X	x					
#8	X				X			
#9						X		
#10								
#11								
#12						X		
#13								X

Table 3 Splitting tension strength data

Core/sample	Splitting tension strength, psi
#2 New	330
#2 Old	580
#3 Old	370
#8 Old A	380
#8 Old B	240
#8 Old C	350
Average Old	380
Average #8	320

Table 4 Compressive strength data

Core/sample	Compression strength, psi
#1 Old	4740
#3 Old	6960
#4 Top	6560
#4 Bottom (Rib/Web)	4730
#7 Rib/Web	5890
Average Old	5780

Table 5 Tension and compression comparison data

Core/Sample	Splitting tension	Compression	Ratio Tension/Compression
#2 Old	580	5780[a]	0.100
# 3 Old	370	5780[a]/6960	0.064/0.053
# 8 Old Average	323	5780[a]	0.055

Note: [a] average all Old

Table 6 Unit weight data

Core/sample	Gs	Unit Weight, lb/ft^3	Absorption, percent (%)
#4 Top	2.28	142.2	2.4
#4 Bottom (Rib)	2.23	139.4	3.6

Table 7 Elastic modulus data

Core/sample	Elastic Modulus, psi	ACI: Estimate of E^a, psi	Ratio
#4 Top	4075684		
	4193791		
	Average 4.13×10^6	4.53×10^6	0.913
#4 Bottom (Rib)	3625171		
	3671902		
	Average 3.65×10^6	3.74×10^6	0.976
#7 Rib	3857110		
	3932754		
	Average 3.89×10^6	4.17×10^6	0.934
	Average Rib 3.77×10^6	3.96×10^6	0.955

Note: [a] $E = \text{unit weight}^{1.5} \times f_c'^{1/2}$ (see Tables 4 and 6)

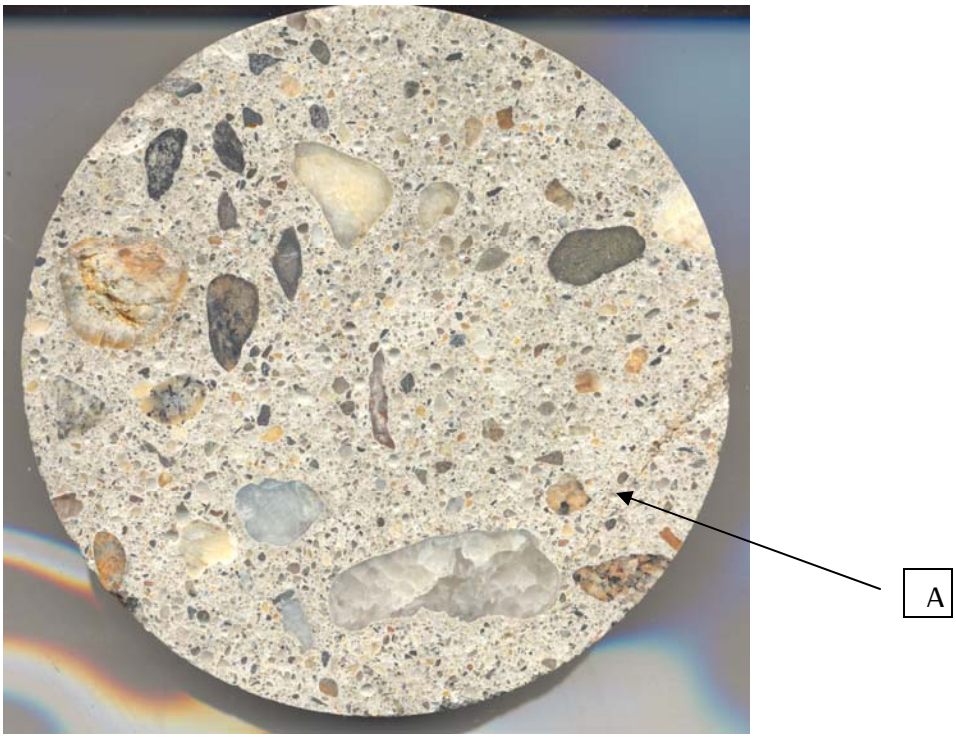

Figure 1 Core # 1 polished surface of top

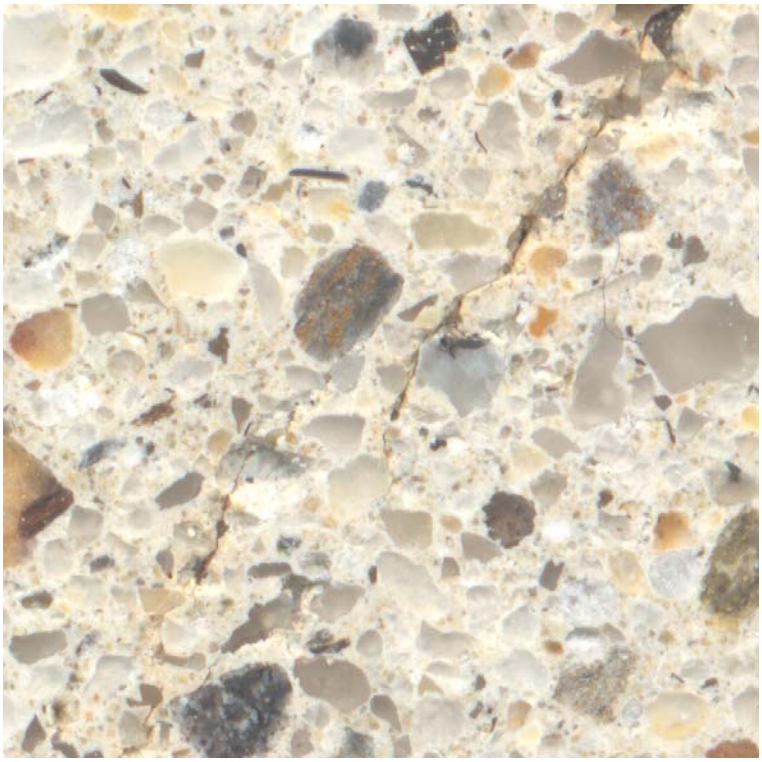

Figure 2 Section A close up of Figure 1 core #1

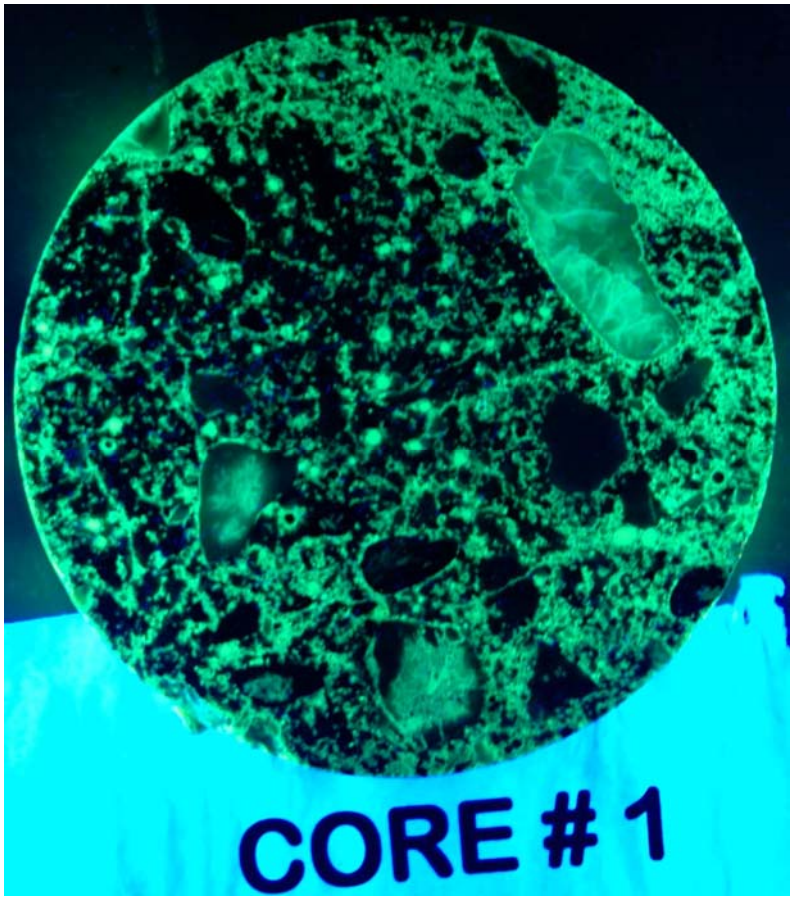

Figure 3 Core #1 polished and coated with impregnated epoxy under UV to enhance microcracks

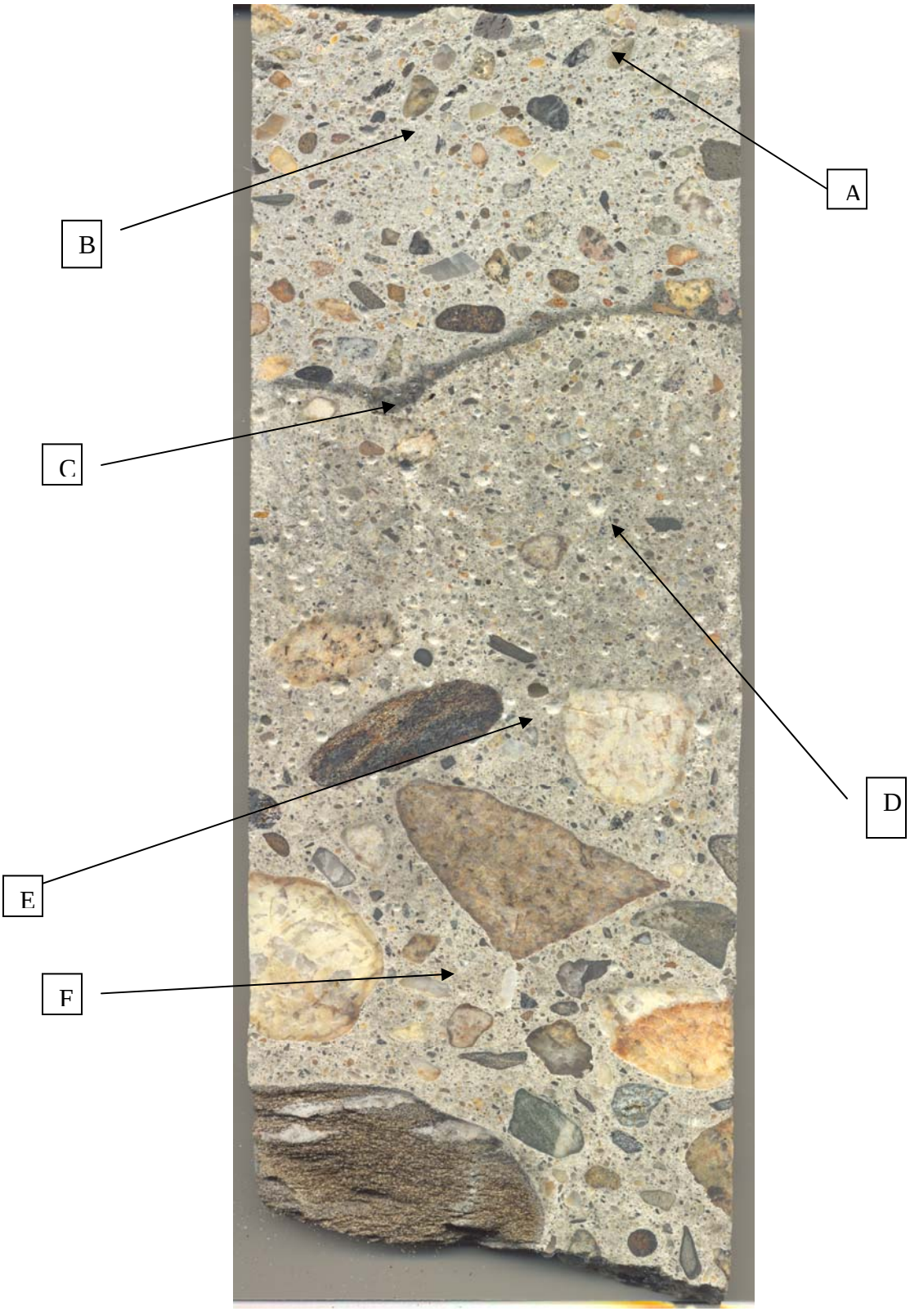

Figure 4 Core # 5 polished surface

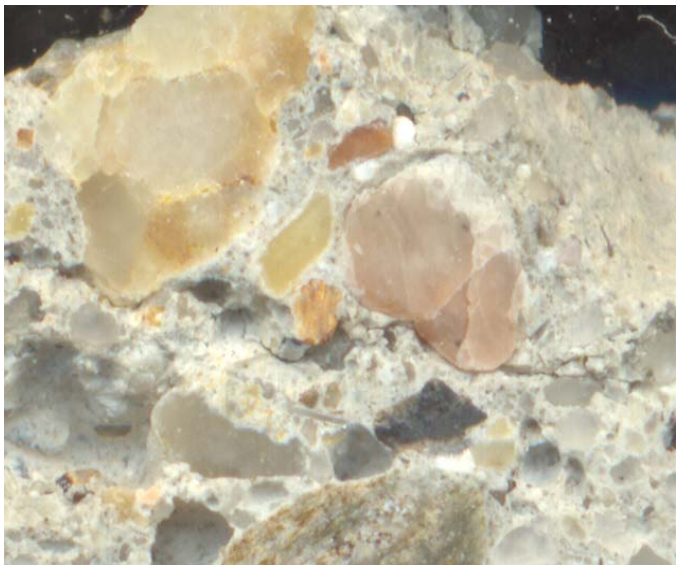

Figure 5 Section A close up of Figure 4 core #5

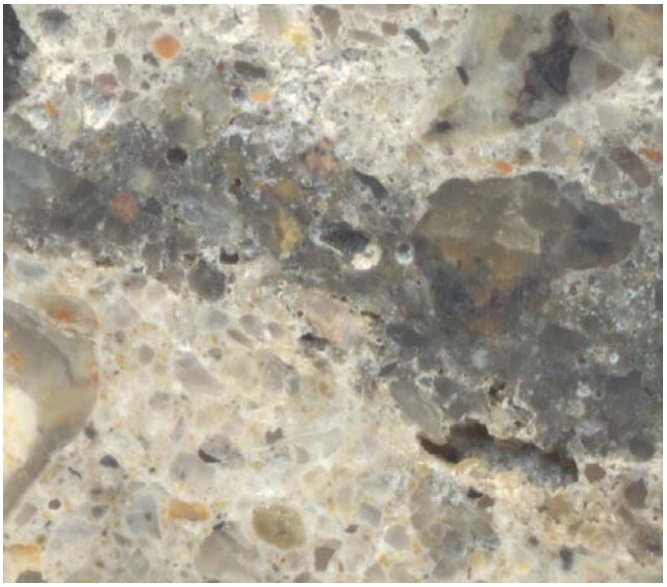

Figure 6 Section C close up of Figure 4 core #5

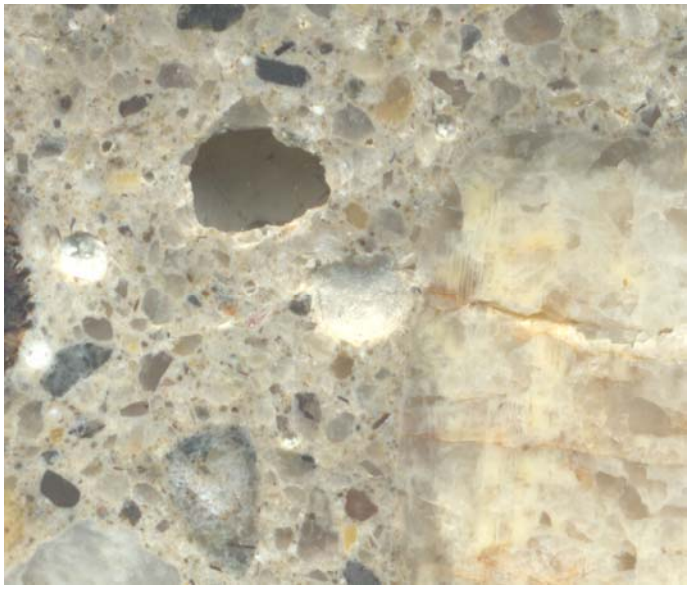

Figure 7 Section E close up of Figure 4 core #5

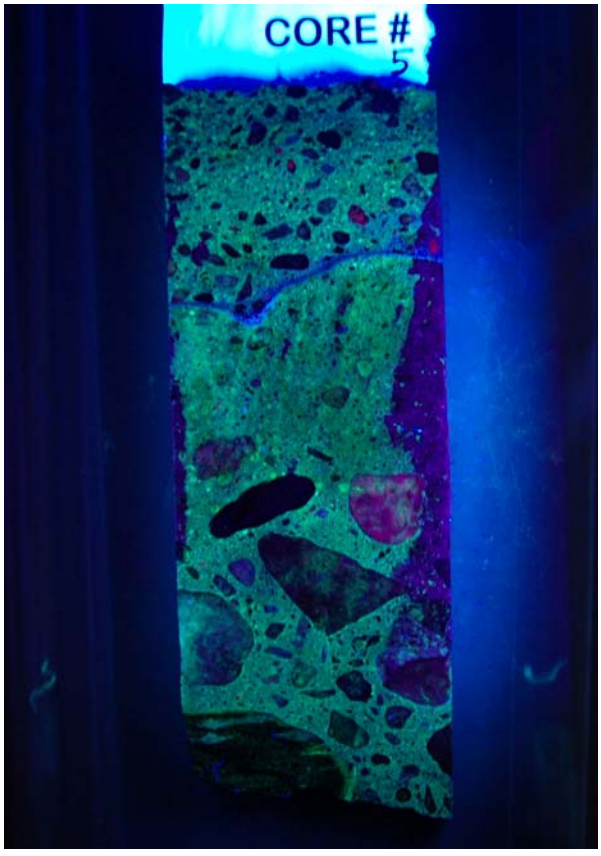

Figure 8 Core 5 polished section coated with impregnated epoxy and viewed under UV

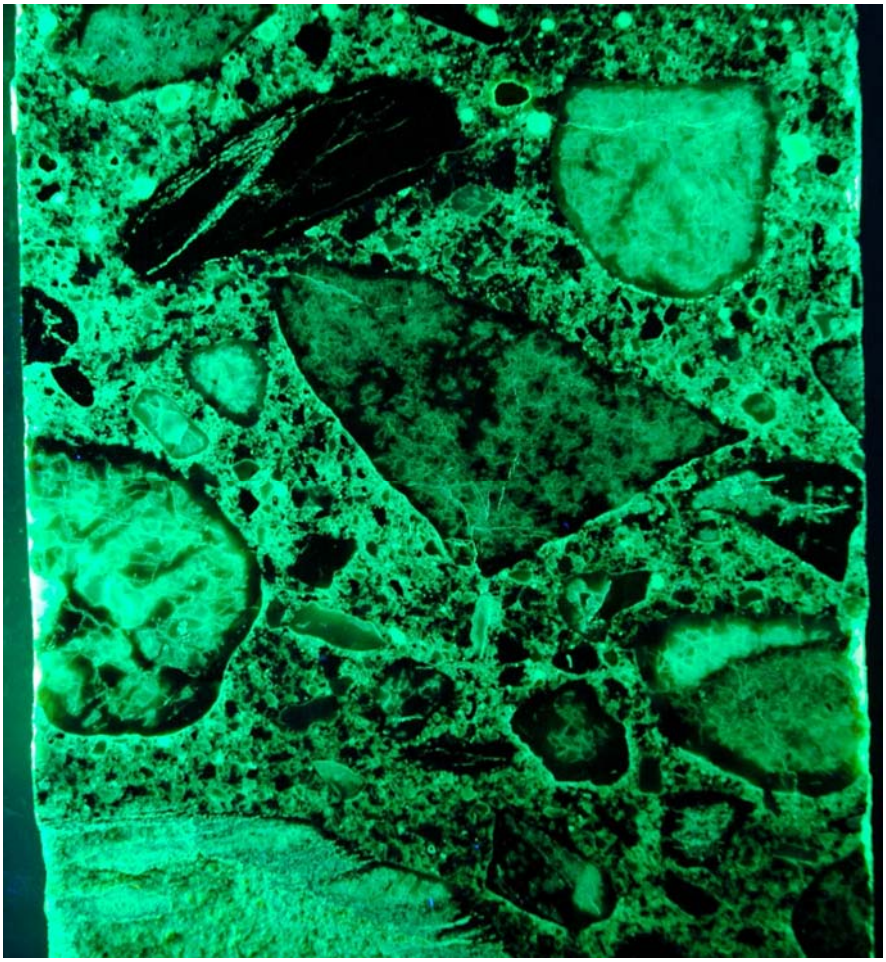

Figure 9 Core 5 polished mid section coated with impregnated epoxy under UV to emphasize micro cracks (see Figures 4, 7 and 8)

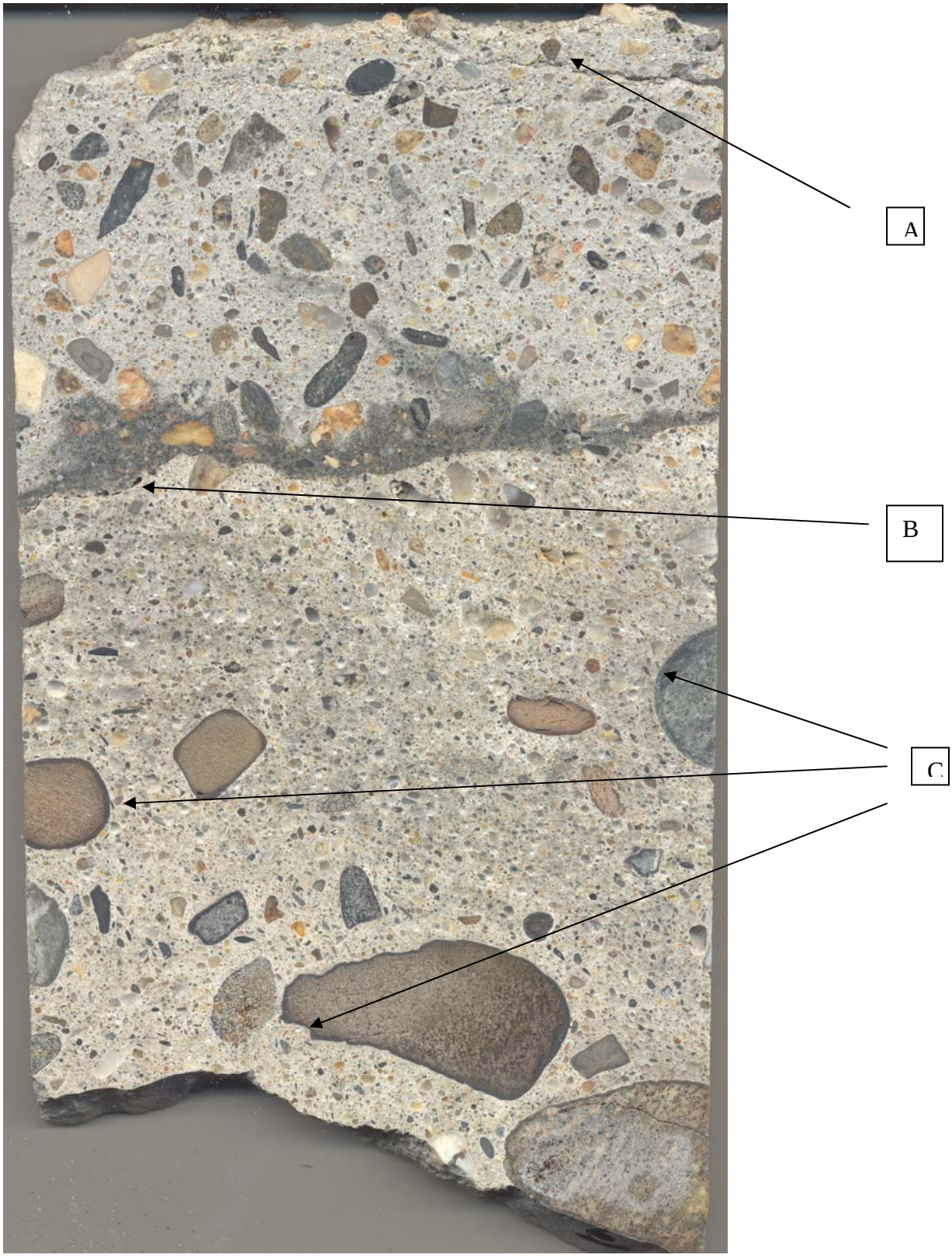

Figure 10 Core # 6 showing polished surface

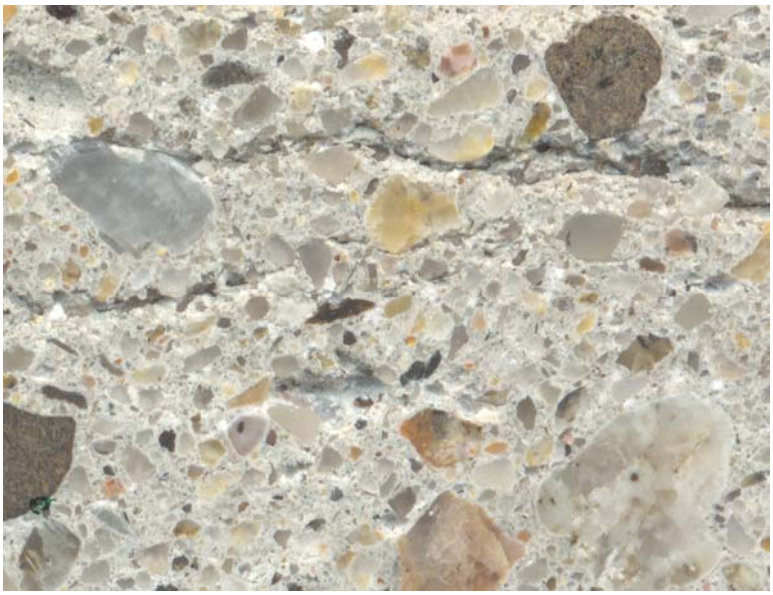

Figure 11 Section A of Figure 10 of Core # 6

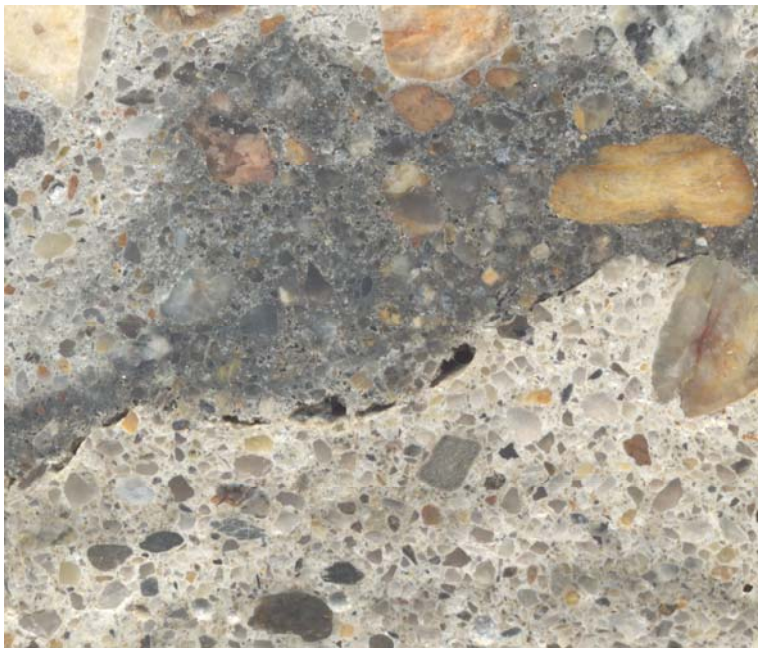

Figure 12 Section B of Figure 10 Core # 6

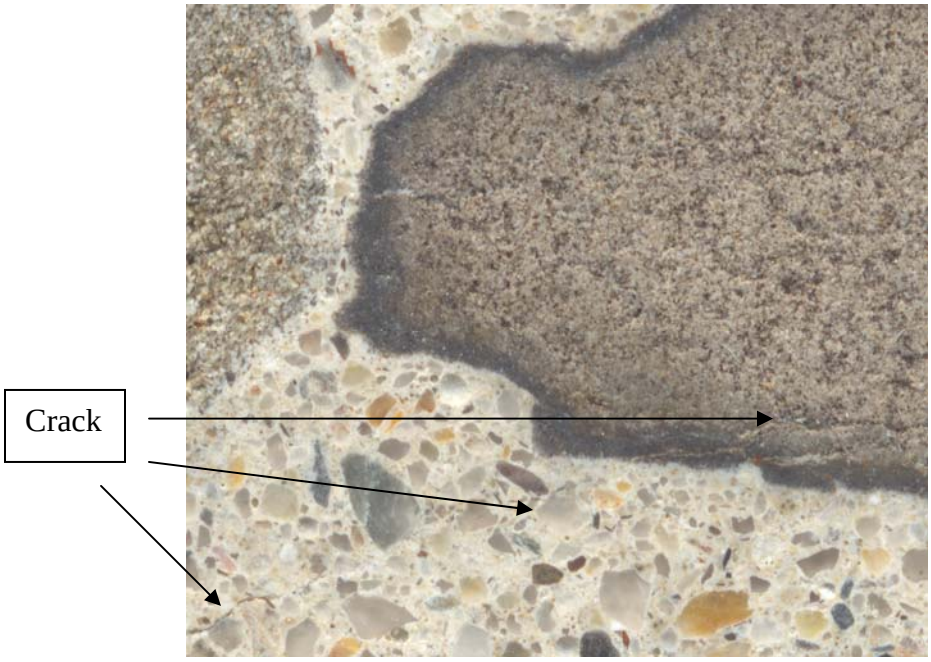

Figure 13 Section C of Figure 10 Core # 6

Figure 14 Polished section of Core # 9

Figure 15 Section A close up of Figure 14 Core #9

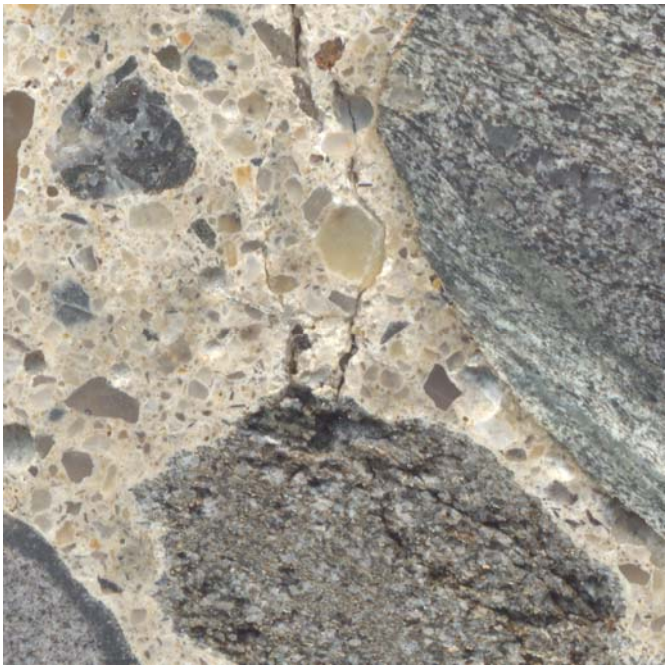

Figure 16 Section B close up of Figure 14 core #9

Figure 17 Section C close up of Figure 14 core #9

Figure 18 Section D close up of Figure 14 core #9

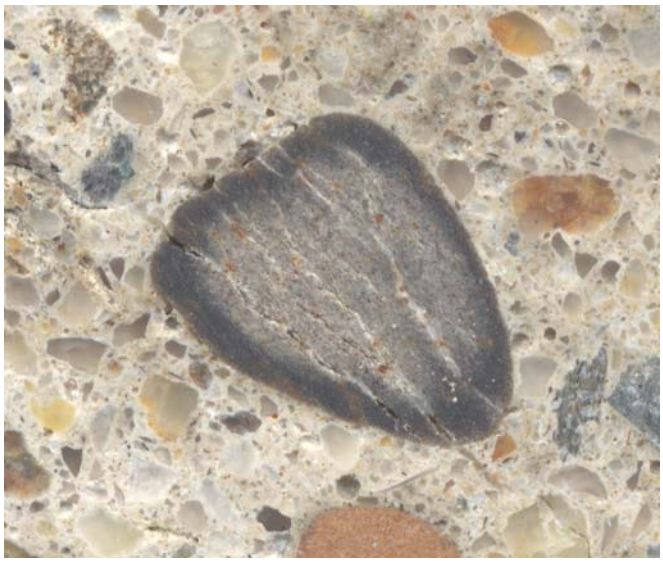

Figure 19 Section E close up of Figure 14 core #9

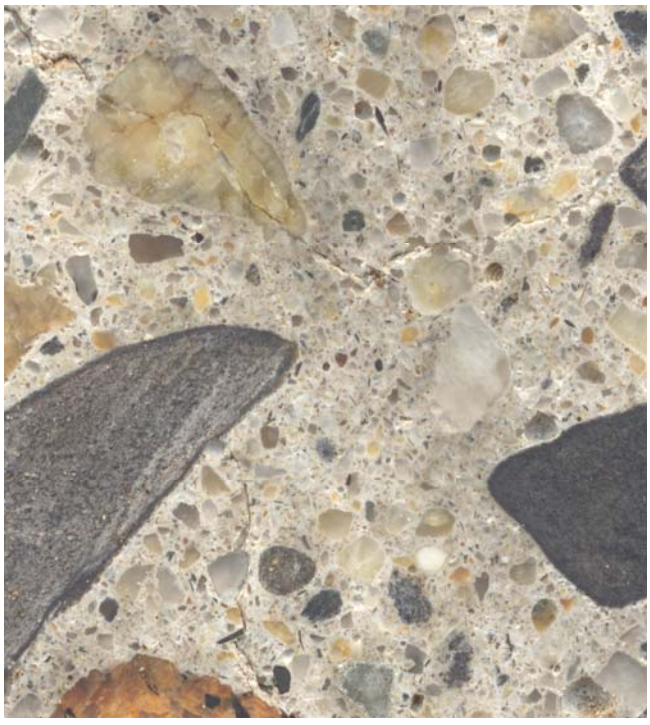

Figure 20 Section F close up of Figure 14 core #9

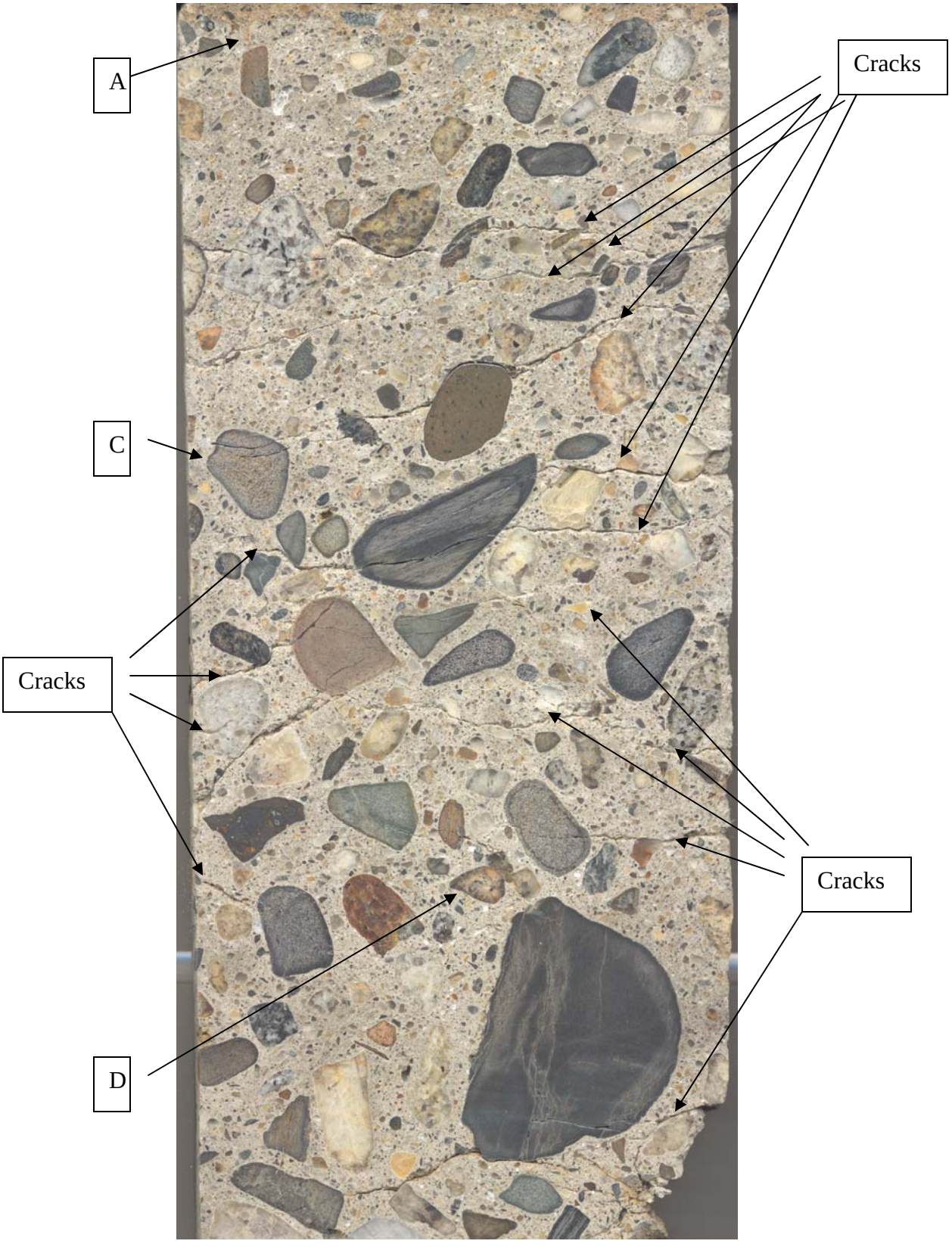

Figure 21 Polished surface of core #12

Figure 22 Section A of Figure 21 core #12

Figure 23 Section C of Figure 21 core #12

Figure 24 Section D of Figure 21 core #12

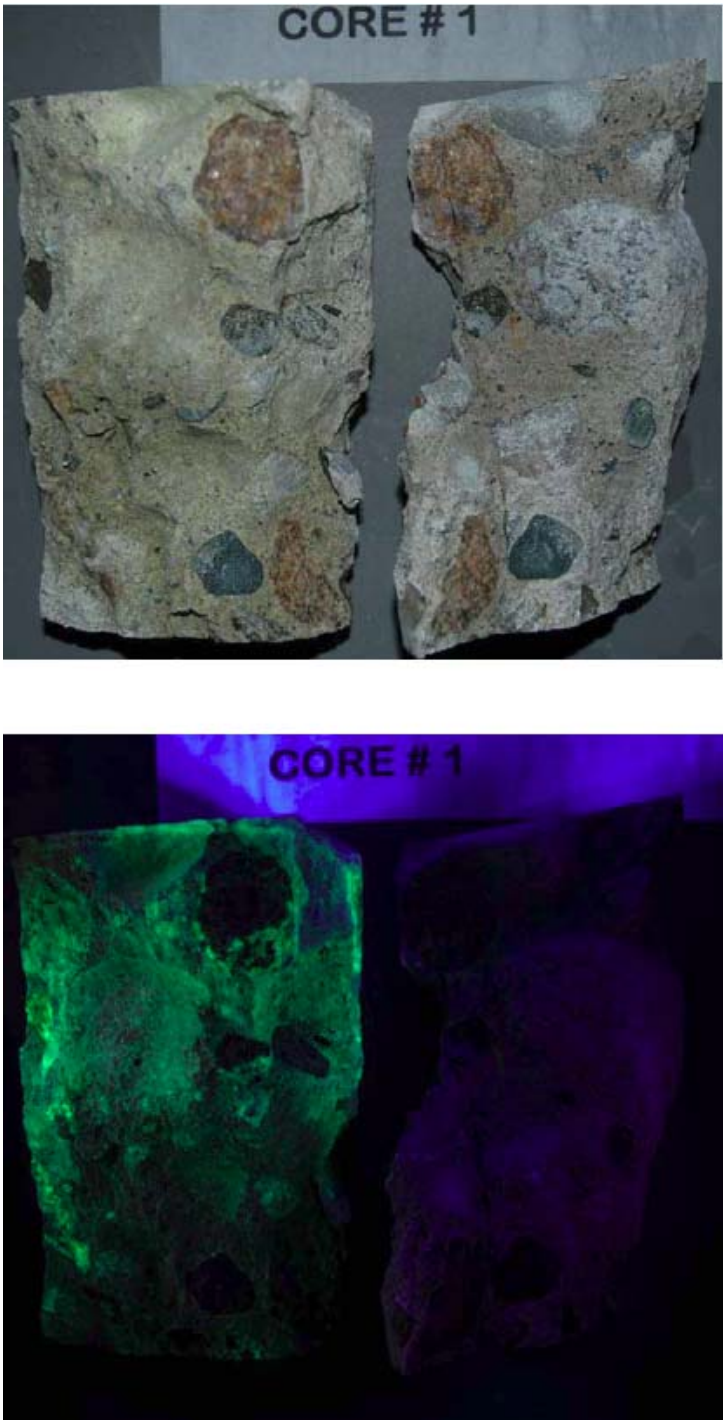

Figure 25 Core #1 compression sample treated with Uranyl acetate dihydrate (left side) under normal light (top) and ultra violet light (bottom)

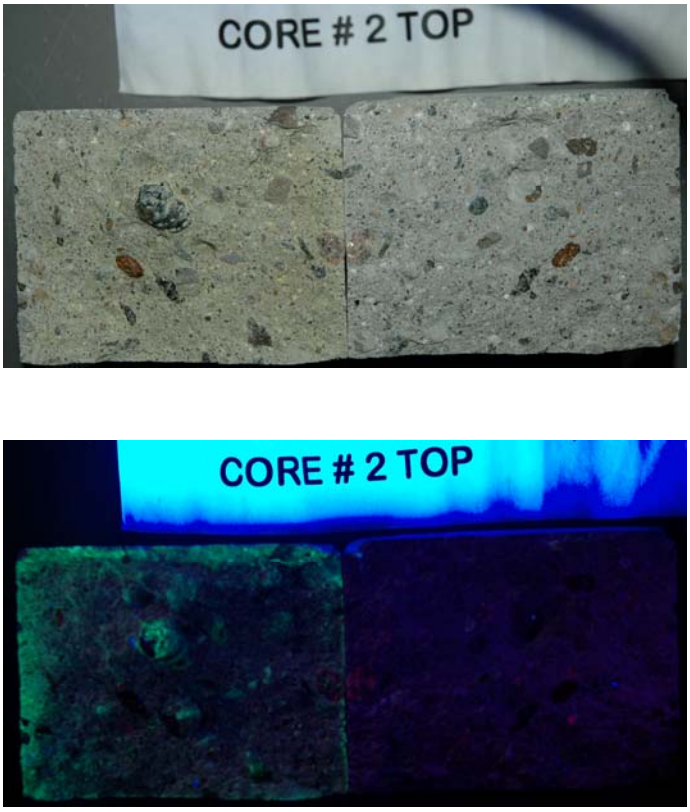

Figure 26 Core #2 tensile sample treated with Uranyl acetate dihydrate (left side) under normal light (top) and ultra violet light (bottom)

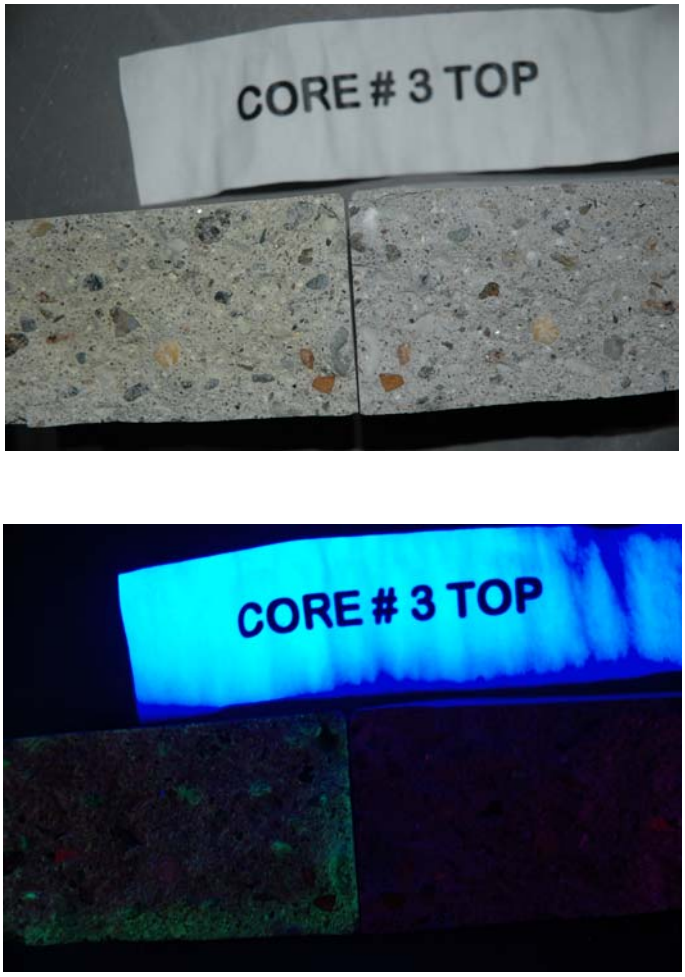

Figure 27 Core #3 Top tensile sample treated with Uranyl acetate dihydrate (left side) under normal light (top) and ultra violet light (bottom)

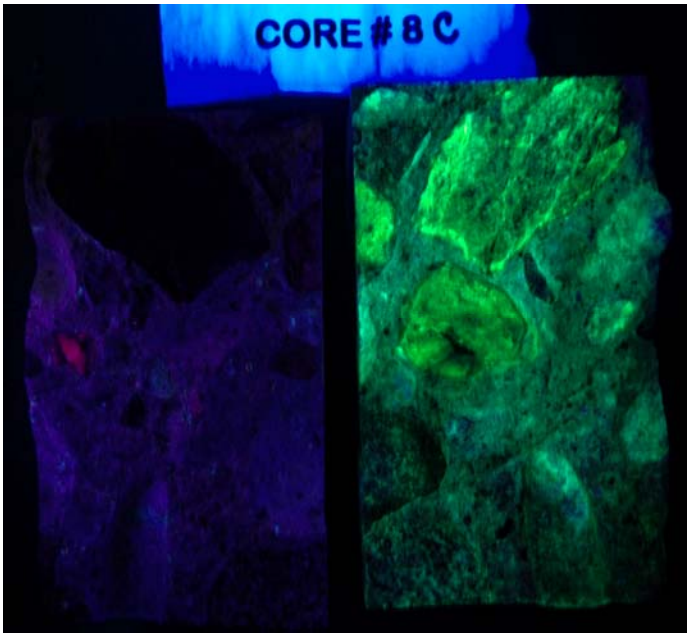

Figure 28 Core # 8C tensile sample treated with Uranyl acetate dihydrate (right side) under normal light (top) and ultra violet light (bottom)

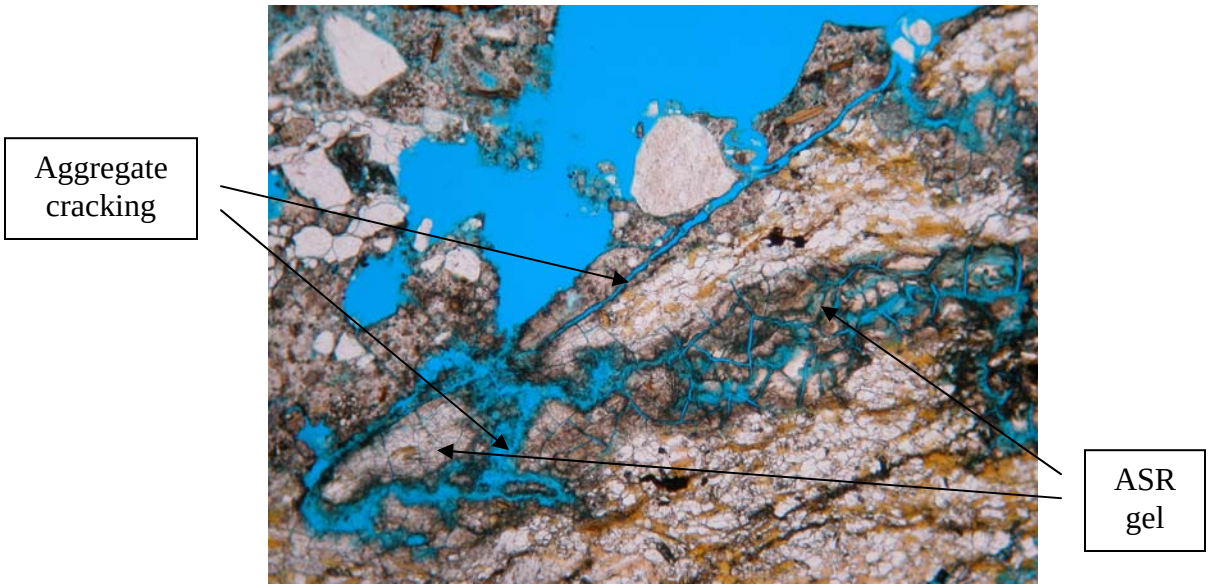

Figure 29 Core 13 vertical section showing ASR gel inside cracked granite coarse aggregate

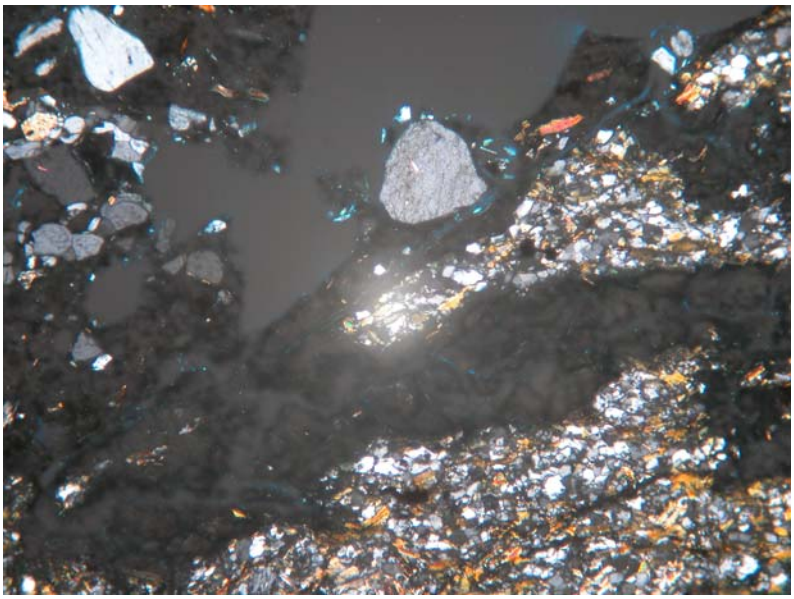

Figure 30 Core 13 vertical section showing amorphous gel (dark portion)

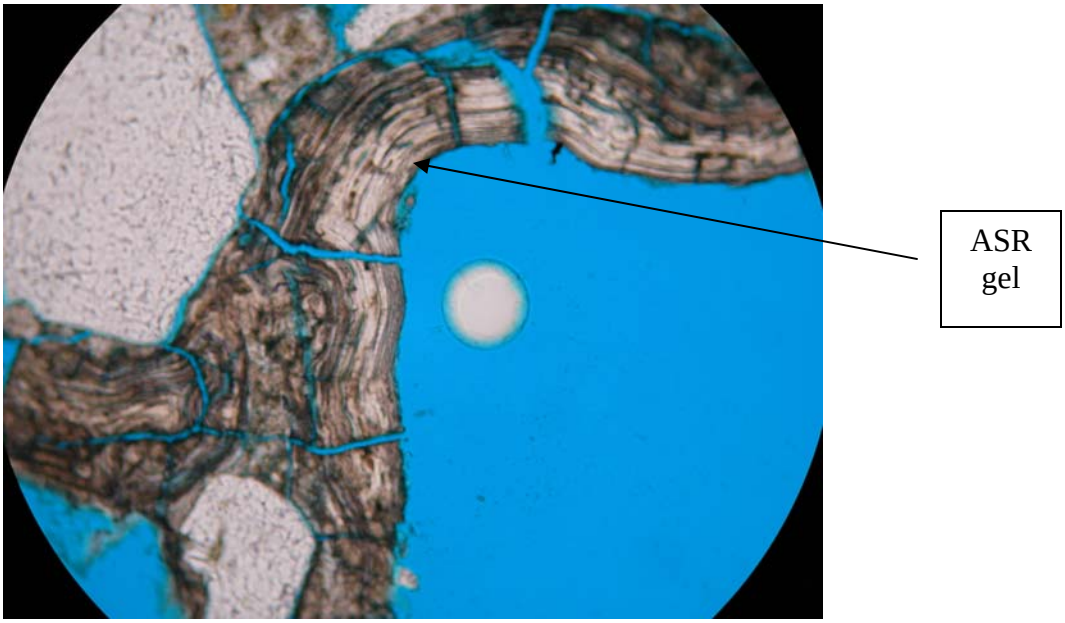

Figure 31 Core 13 vertical section showing layered ASR gel at the edges of a crack

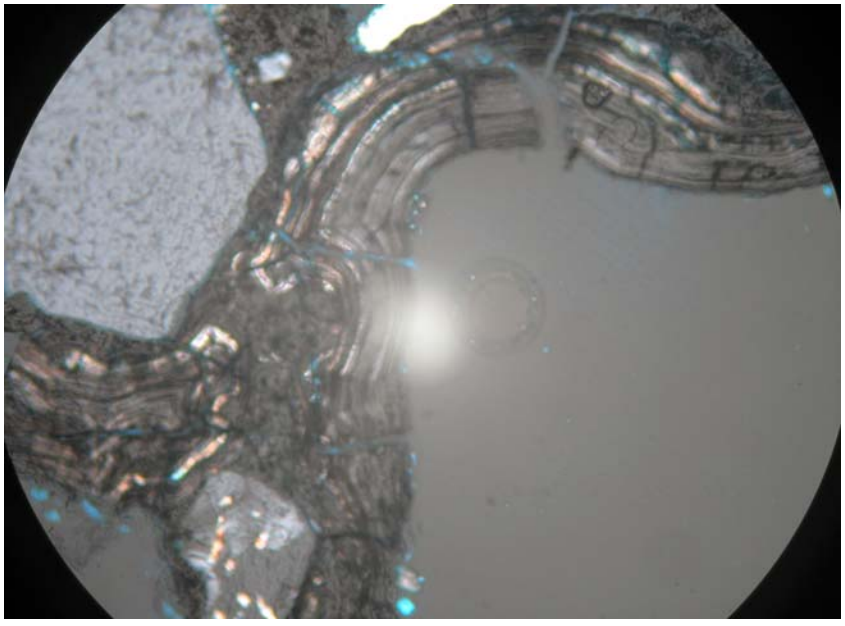

Figure 32 Core 13 vertical section showing the alternate layers of crystalline (colored portion) and non-crystalline gel (dark colored) under crossed polarized light (see Figure 31)

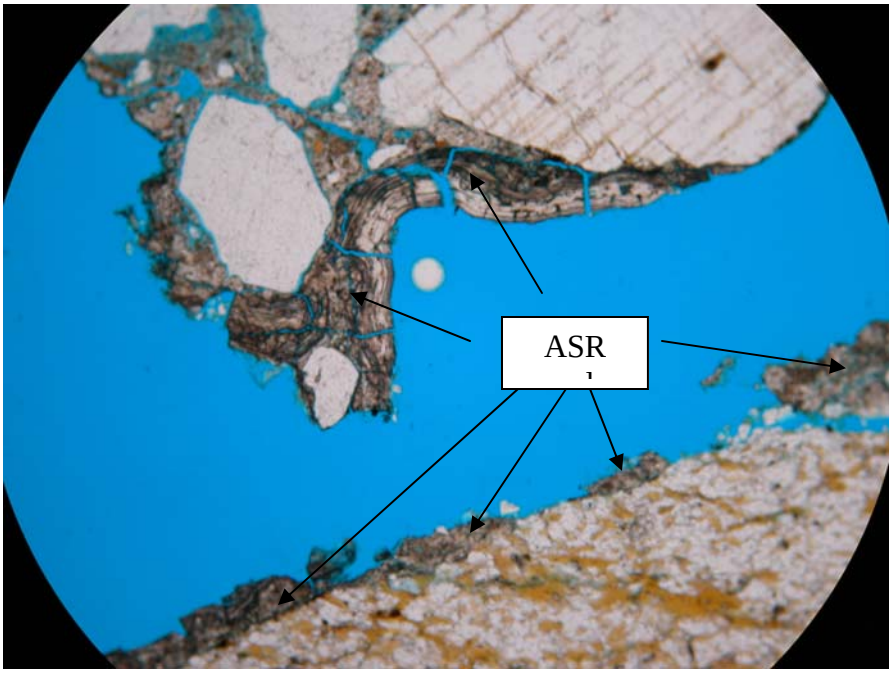

Figure 33 Core 13 vertical section showing a lower magnification view of Figure 31 and 32

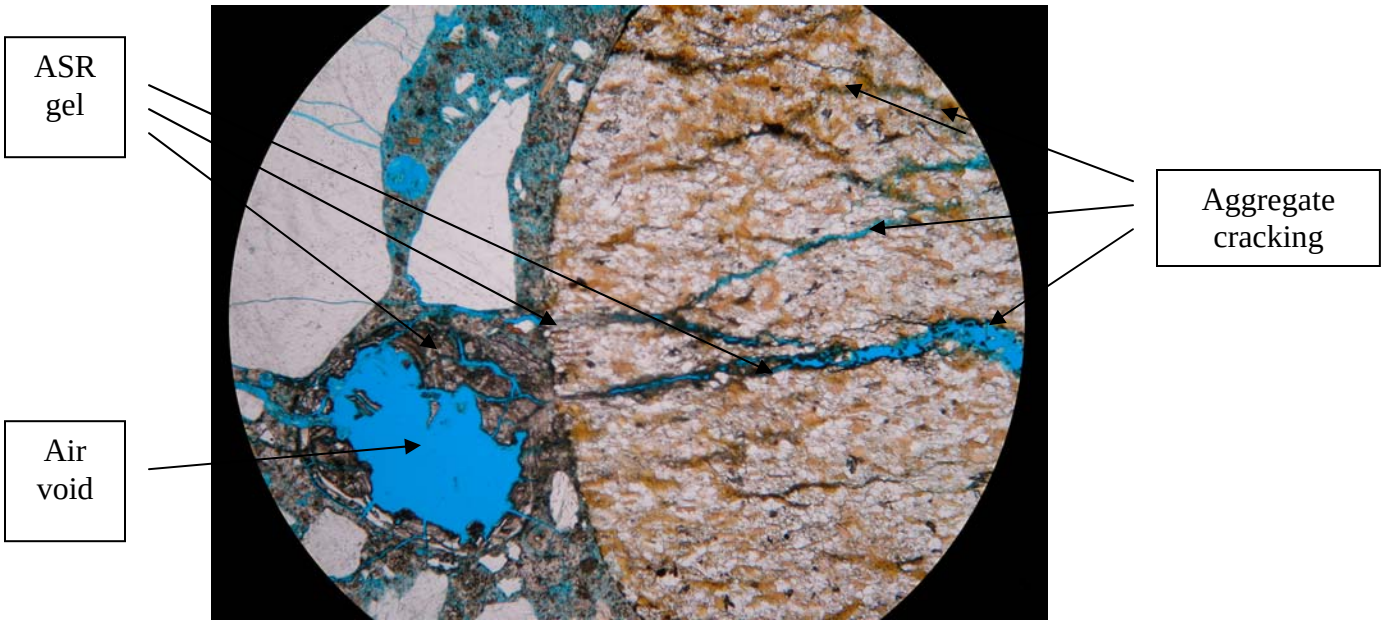

Figure 34 Core 13 vertical section showing aggregate cracking, ASR gel

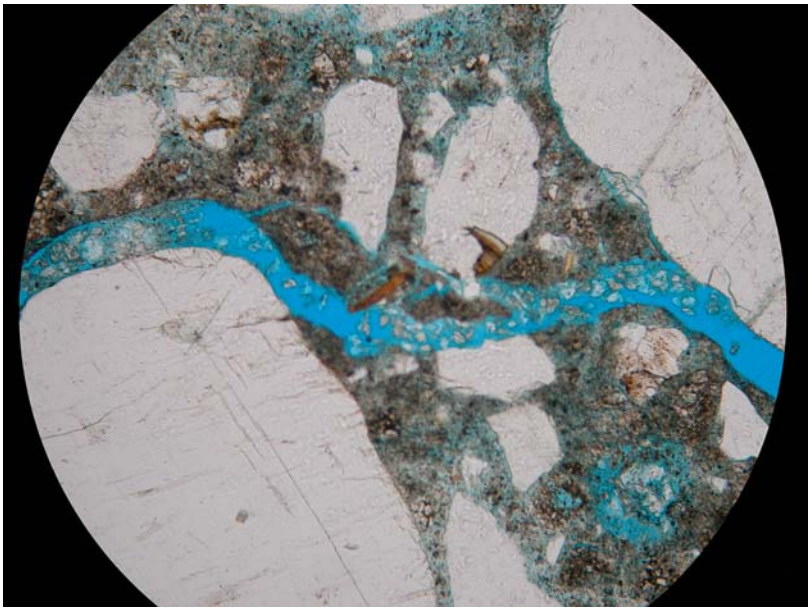

Figure 35 Core 13 vertical section showing Ettringite along the crack at the aggregate-paste interfaces

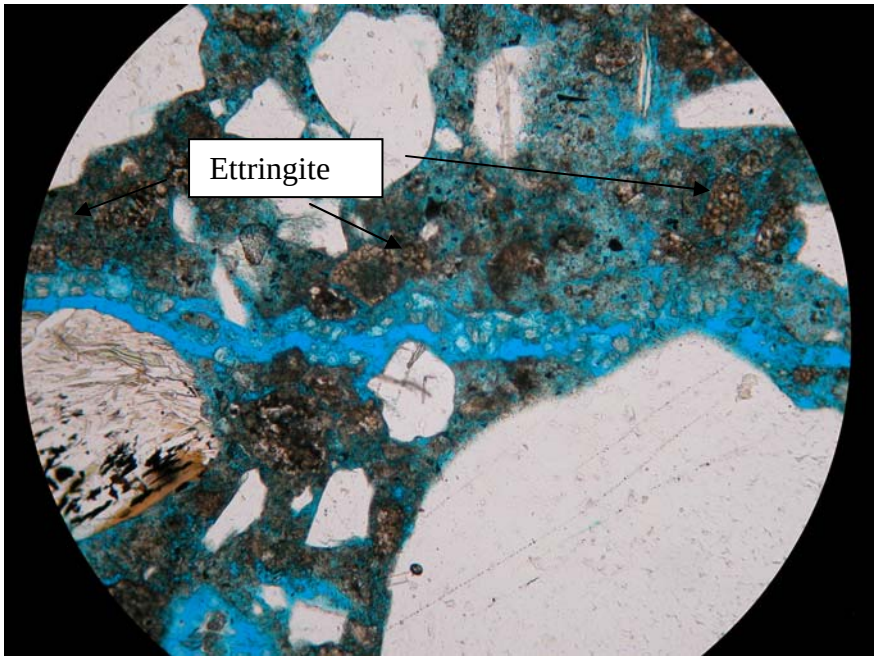

Figure 36 Core 13 horizontal section showing secondary ettringite

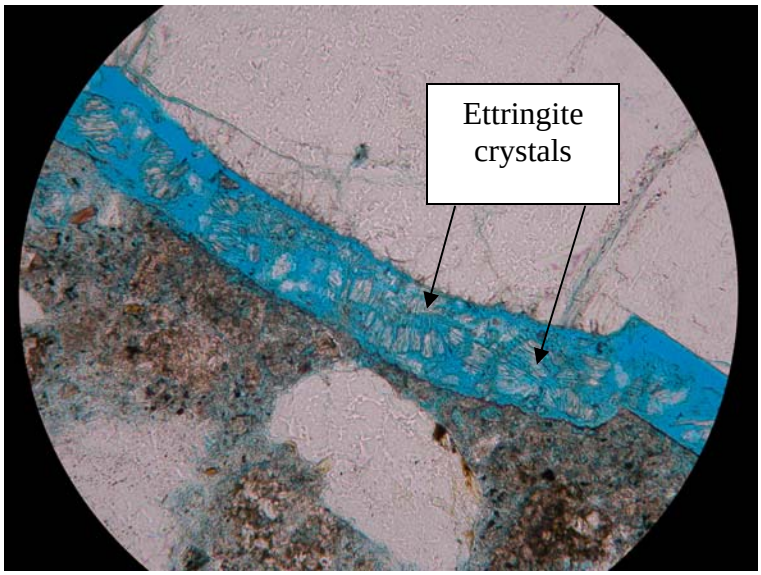

Figure 37 Core 13 horizontal section showing enlarged view of Figure 36

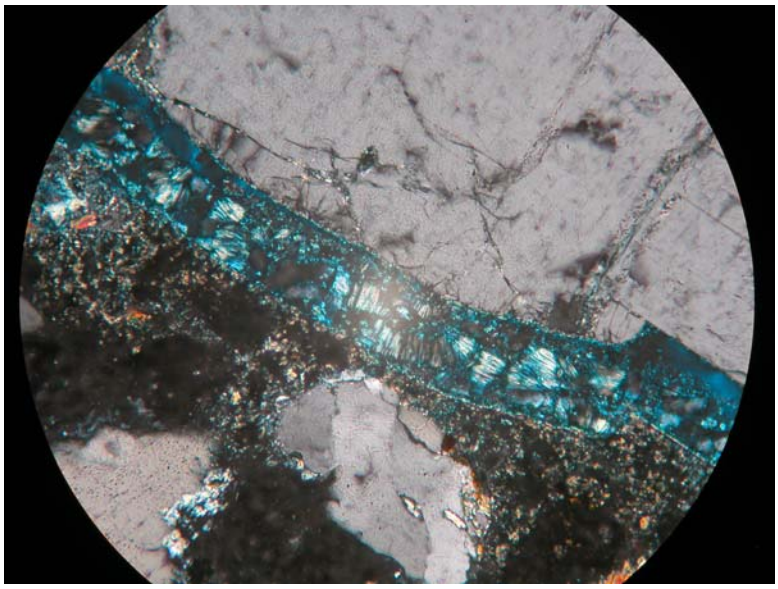

Figure 38 Core 13 horizontal section showing cross polarized light (see Figure 37)

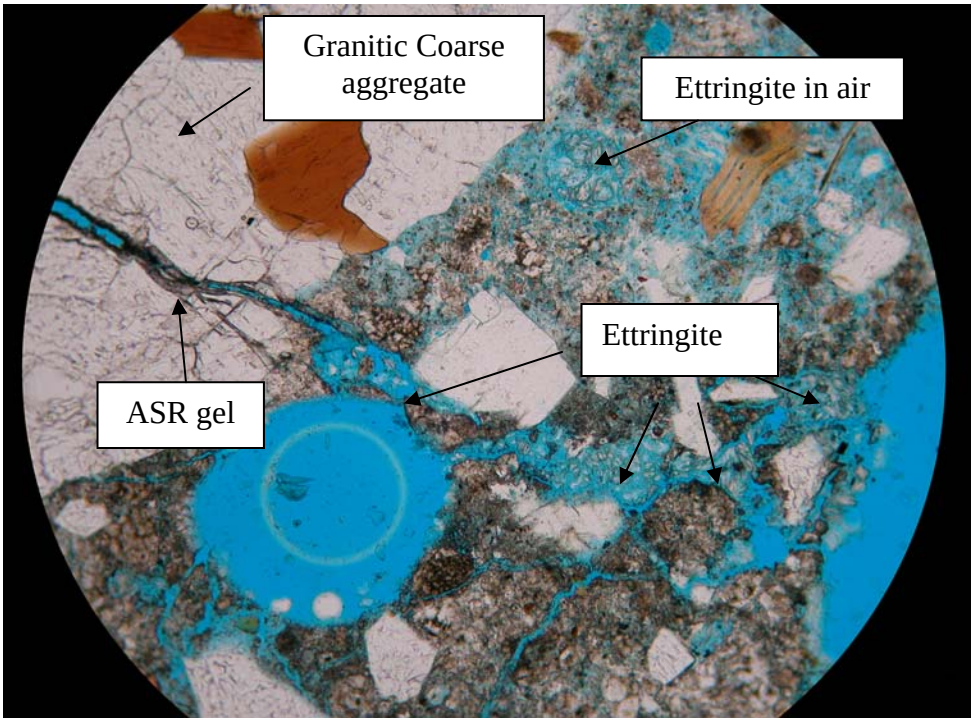

Figure 39 Core 13 horizontal section showing ASR and secondary Ettringite

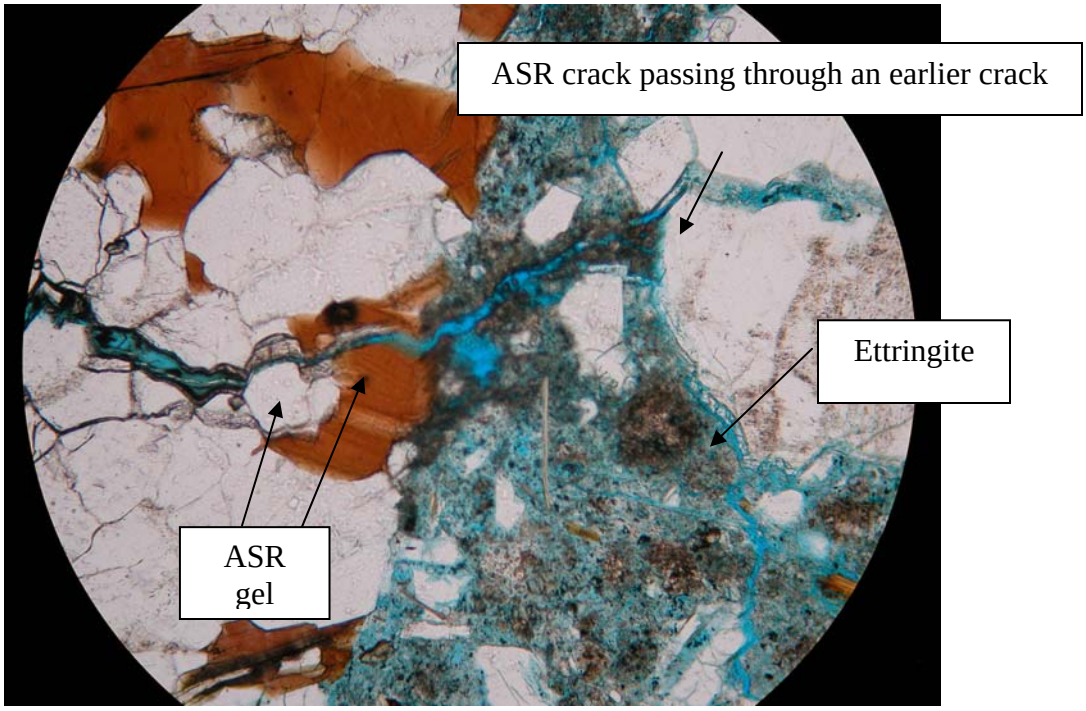

Figure 40 Core 13 horizontal section showing ASR and DEF in the same place

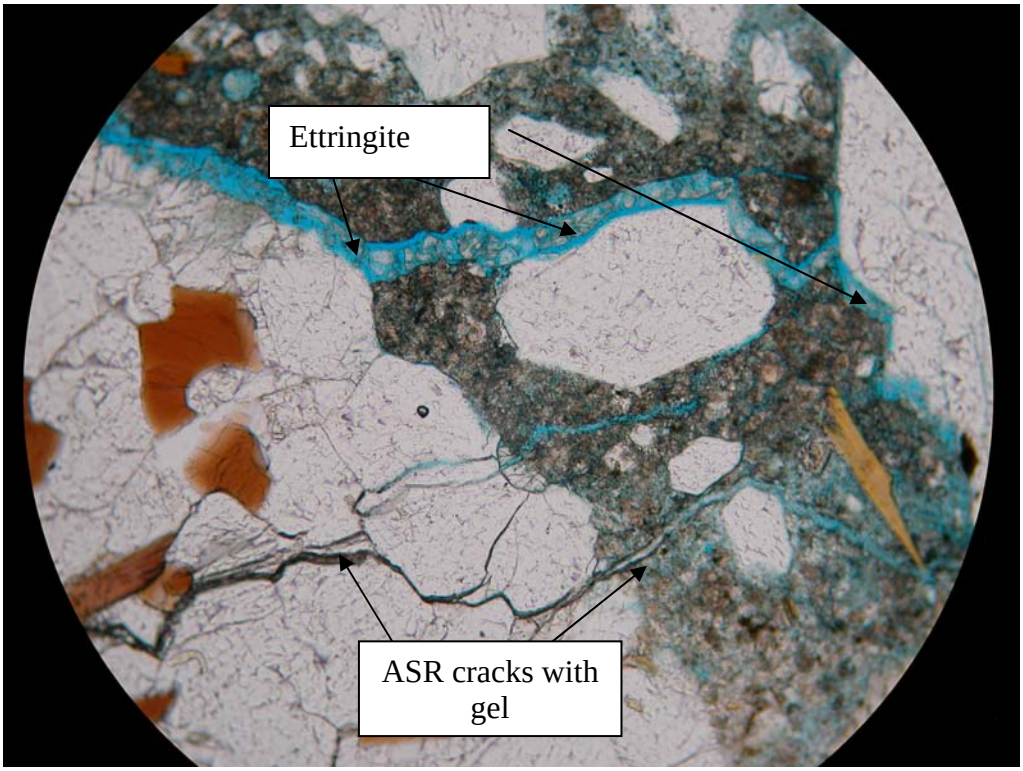

Figure 41 Core 13 horizontal section showing ASR and Ettringite

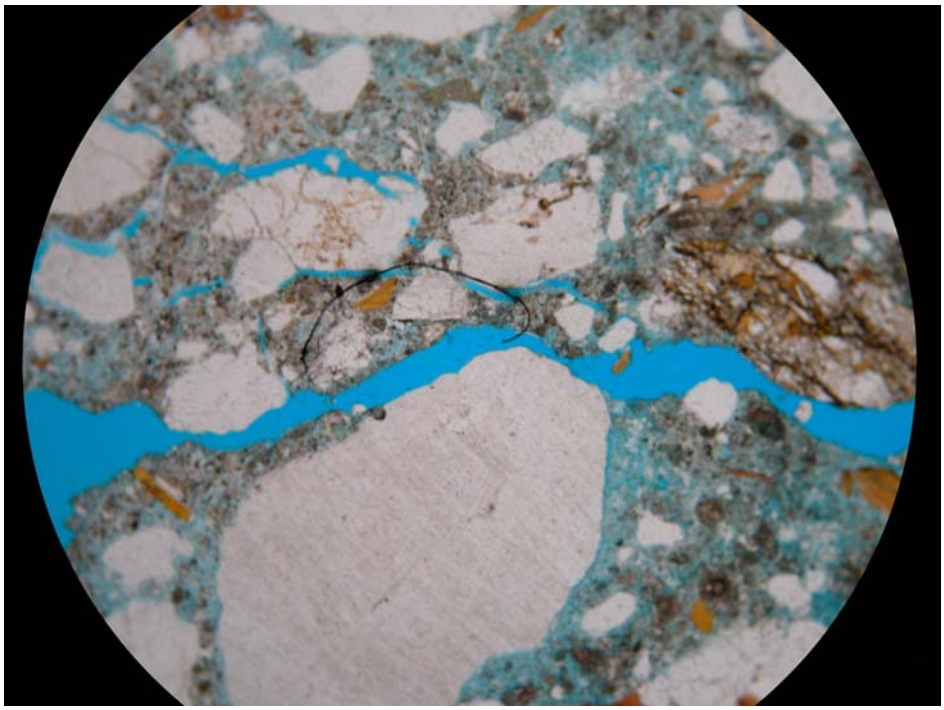

Figure 42 Core 13 horizontal section showing Typical crack pattern

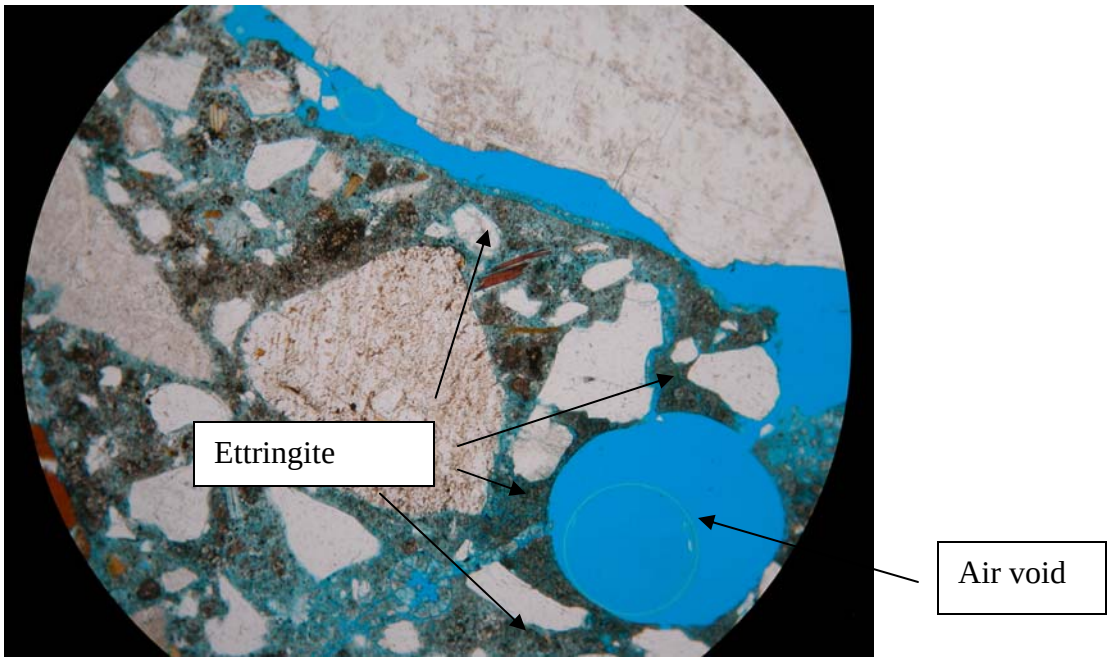

Figure 43 Core 13 horizontal section showing Another example of crack pattern

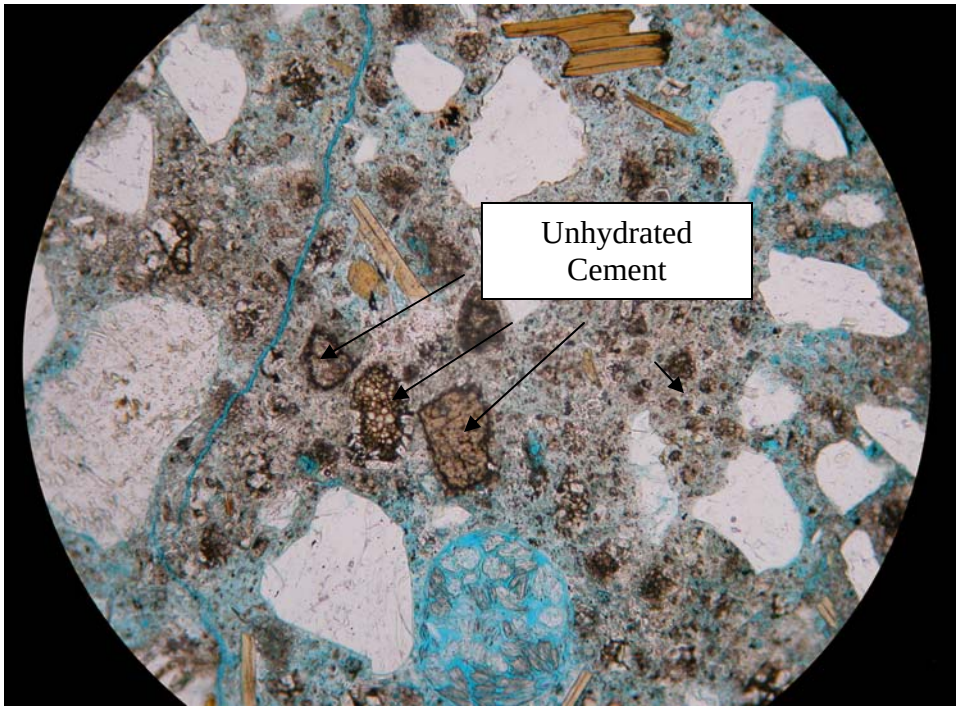

Figure 44 Core 13 horizontal section showing large number of unhydrated, coarser portland cement particles typical of Rosendale cement.

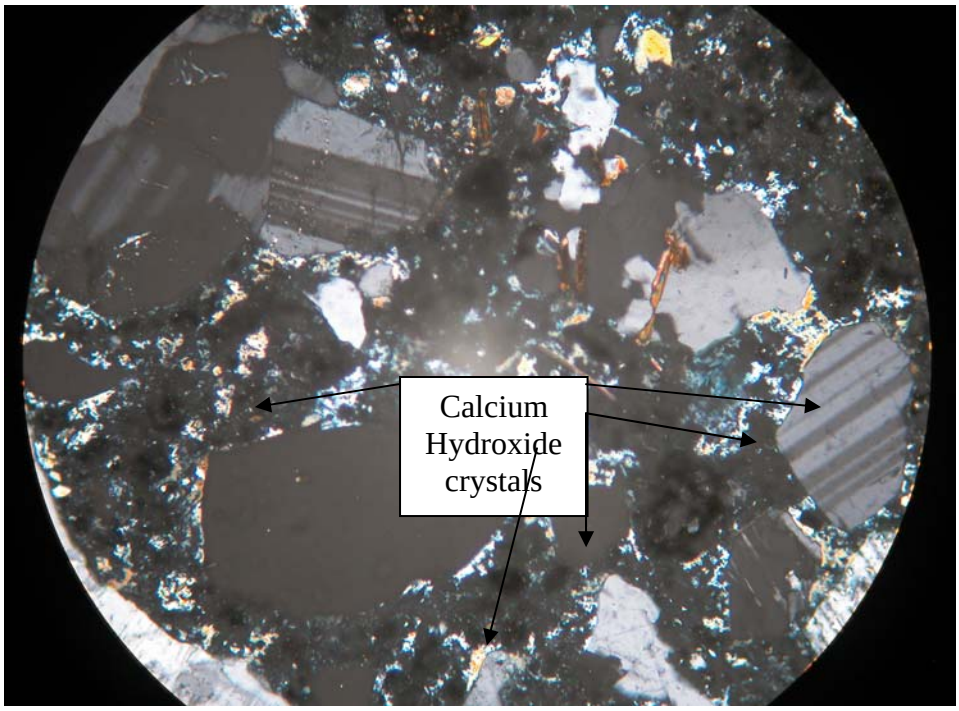

Figure 45 Core 13 horizontal section showing well crystallized, coarser calcium hydroxide crystals at the aggregate-paste interfaces as well as in the matrix.